water

MDPI

Article

Delineating the Potential Areas of Rainwater Harvesting in Arid Regions Using Remote Sensing and GIS Techniques

Mohamed Abdelkareem [1,2,*], Abbas M. Mansour [1] and Ahmed Akawy [1]

[1] Geology Department, South Valley University, Qena 83523, Egypt
[2] Remote Sensing Lab., South Valley University, Qena 83523, Egypt
* Correspondence: mohamed.abdelkareem@sci.svu.edu.eg

Abstract: Remote sensing (RS) data have allowed prospective zones of water accumulation (PZWA) that have been harvested during rainstorms to be revealed. Climatic, hydrologic, and geological data have been combined with radar and optical remote sensing data. A wide array of remote sensing data, including SRTM, Sentinel-1&2, Landsat-8, TRMM, and ALOS/PALSAR data, were processed to reveal the topographical characteristics of catchments (elevation, slope, curvature, and TRI) and geological (lineaments, lithology, and radar intensity), hydrological (Dd, TWI, and SPI), ecological (NDVI, InSAR CCD), and rainfall zones in Wadi Queih (WQ), which is an important drainage system that drains into the Red Sea. Radar data improved the structural elements and showed that the downstream area is shaped by the northeast–southwest (NE-SW) fault trend. After giving each evidential GIS layer a weight by utilizing a GIS-based, knowledge-driven methodology, the 13 GIS layers were integrated and combined. According to the findings, the studied basin can be classified into six zones based on how water resources are held and captured, which are very low, low, moderate, high, very high, and excellent. These zones correspond to 6.20, 14.01, 21.26, 36.57, 17.35, and 4.59% of the entire area. The results suggested a specific location for a lake that can be used to store rainwater, with a capacity of ~240 million m^3 in the case of increasing rainfall yield. Such a lake complements the present lake at the end of WQ, which can hold about 1 million m^3. InSAR coherence change detection (CCD) derived from Sentinel-1 data revealed noticeable changes in land use/land cover (LU/LC) areas. Areas that displayed changes in surface water signatures and agricultural and human activities were consistent with the predicted very high and excellent zones. Thus, the predicted model is an important approach that can aid planners and governments. Overall, the integration of optical and radar microwaves in RS and GIS techniques can reveal promising areas of rainwater and water accumulation.

Keywords: remote sensing; GIS; modeling; rainwater harvesting

check for updates

Citation: Abdelkareem, M.; Mansour, A.M.; Akawy, A. Delineating the Potential Areas of Rainwater Harvesting in Arid Regions Using Remote Sensing and GIS Techniques. *Water* **2023**, *15*, 3592. https://doi.org/10.3390/w15203592

Academic Editors: Isabel Banos-González, Adriana Bruggeman and Pedro Pérez-Cutillas

Received: 3 August 2023
Revised: 18 September 2023
Accepted: 21 September 2023
Published: 13 October 2023

1. Introduction

Water resources are needed for the expansion of agricultural, urban, and industrial activities. Population growth, along with numerous environmental, social, economic, and climate change factors, is causing increased demand for freshwater supplies, which is the biggest obstacle to reaching the goals of sustainable development [1–3]. Future water availability in many locations is subject to significant uncertainty due to climate change [4]. Climate change will have an impact on precipitation, runoff, snowmelt, and groundwater recharge, in addition to having an impact on hydrological systems, water quality, and temperature. Therefore, it will cause droughts and storms and increase water shortages in developing countries, which will affect the agriculture sectors (IPCC. 2014b). Furthermore, in coastal places, increases in sea level will have an impact on the salinity of surface water and groundwater [4,5]. Accordingly, water supplies around the world are becoming diminished, endangering human and environmental health as well as sustainable development [6,7]. Therefore, securing water resources through rainwater harvesting is a critical issue.

In arid and semi-arid places where there is a scarcity of water and where water sources are not accessible or too expensive to develop and utilize, collecting rainwater, also known as rainwater harvesting (RWH), is a strategy for increasing surface water resources to increase the quantity and quality of water available to the inhabitants [8] and alleviating drought [9]. Rainwater harvesting (RWH) includes the collection of the water captured during storms [10] in ponds, lakes, etc., with or without the groundwater infiltrated into the soil. The rainwater harvesting system's surface acts as the region of catchment because it directly collects rainfall and supplies the system with water during storms [11]. Such captured rainwater can be employed in irrigating plants and can provide people and animals with water for use in their lives in arid regions [12]. Furthermore, RWH can reduce surface runoff and flash flood hazards [13,14].

Hydrologic modeling is necessary to address and prevent the depletion and scarcity of water resources [15–18]. For water resource research and estimation and the global assessment of groundwater events, remote sensing (RS) and GIS techniques are beneficial instruments [18–22]. In recent years, geospatial methods like GIS and RS have attracted a lot of interest in finding the optimum locations for water harvesting [23–25] and recharging [26]. For the identification of groundwater potentiality, methodologies based on data and knowledge were used [27,28]. To find groundwater resources, a wide array of techniques are employed, such as overlay analysis [17], the analytical hierarchy process (AHP) [29–31], Boolean logic [32], index overlays, and fuzzy methods [33]. Big geographical data can be processed and combined using a GIS technique to anticipate and make it possible to identify new water resources [26]. The GIS-based AHP technique develops a solution to a complex choice analysis and provides valuable information in predicting promising areas [34,35].

Several investigations have effectively modified and evaluated the approach for determining optimum regions for RWH and water accumulation. Several factors can be employed to reveal the optimum areas for RWH, such as the physical characteristics of the terrain, precipitation, LULC, runoff, topographic factors, and soil cover [23,36–38]. Topographic, lithological, climatic, and hydrologic conditions are utilized in probing and modeling the areas of water resources [16,39–44]. Areas with relatively low topography make excellent locations for gathering rainfall, which has historically been used largely for housing and agricultural needs, although there are higher flood hazards [45–48]. In comparison to steep slopes, flat or gently sloping areas hold water [26,34,49], and areas of curvature hold water as well [50]. There are two prominent methods for collecting rainwater: storing it on the surface for later use and recharging groundwater [51]. Additionally, by storing and absorbing rainfall, rainwater harvesting not only enables successful rainwater runoff management [52] but also helps to reduce pollution from non-point sources in metropolitan settings [51,53]. The main supply of groundwater is rainfall that seeps into soil pores in shallow aquifers.

Most of the research in Egyptian deserts was conducted without applying further techniques of RS and GIS to reveal the optimum areas of water resources, and it is becoming necessary to secure such resources through rainwater harvesting in arid regions. Therefore, the goal of the current study is to identify potential water resource locations by utilizing a variety of factors concerning geologic, climatic, topographic, and ecologic data.

2. Study Area

The study area of WQ is a prominent drainage area between Quseir and Safaga cities that covers more than 1890 km^2 (Figure 1). It serves as a significant commercial, industrial, and economic hub, particularly due to its location in the Golden Triangle Area. The known tributaries and wadis are W. Queih, W. Saqi, and W. Abu Aqarib along with hills and mountain areas, e.g., G. Weira, G. Abu Gaharish, G. Kab Amir, G. El-Aradiya, G. Um El-Abas, G. Um Halnami, and G. Abu Aqarib (Figure 2). It is covered by Neoproterozoic crystalline rocks that can be identified and delineated in the eastern and western sectors by NNW and

WNW major normal faults. Compared to impermeable lithologic units, extremely porous lithologic units can hold and capture surface water. The Conoco geological map [54] was applied to digitize the lithologic units. The area consists of ophiolitic rocks, metavolcanics, metasediments, Hammamat sediments, Dokhan volcanics, and Cretaceous/Tertiary rocks that are covered by wadi deposits (Figure 2).

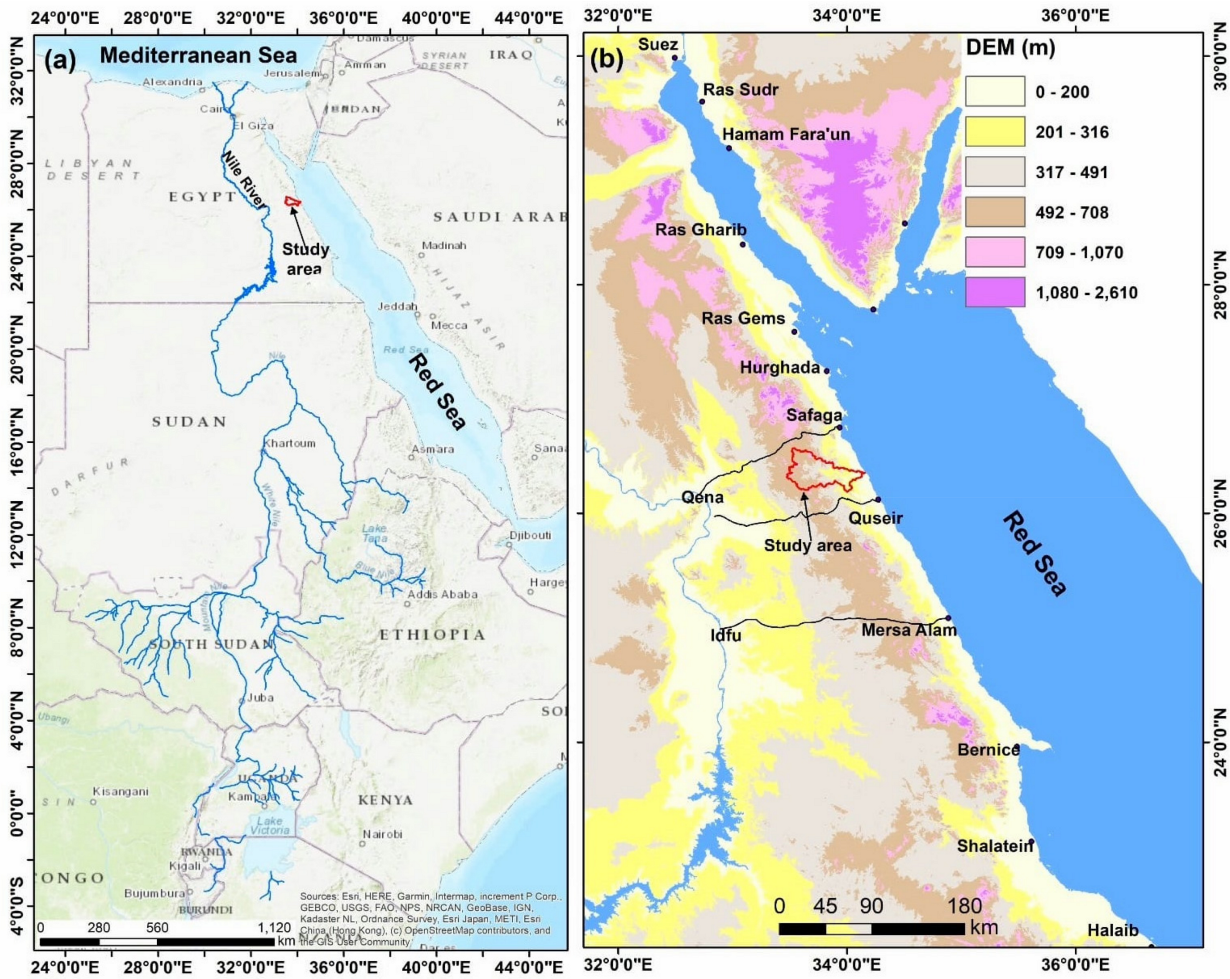

Figure 1. (**a**) Location map of WQ marked with red polygon; (**b**) study area of WQ between Quseir and Safaga along the Red Sea region overlaying the topographic map.

In WQ, variable rainfall and flash floods are the sources recharging groundwater aquifers. Through the loose sediments, this water permeates and gathers on basement depressions or becomes trapped by faults [17,41,55,56]. The average vertical infiltration for the surface soil (aeolian gravel and well-sorted sand) is 5.1 m/day [57]. Rainfall has the capability to permeate strata in large quantities to a high vertical infiltration rate [58]. The WQ basin has a catchment area of around 1800 km^2 and a length of about 67.5 km. Its average width is roughly 26.6 km. The WQ depression runs from northwest to southeast and receives water from the nearby mountains and elevated areas. The area has experienced heavy rainy storms such as those on 6–10 March 2014, 17 January 2010, and 29 December 2010 (Figure 3). On 6 March 2014, the rainfall ranged from 0 to 4.1 mm/day, reached up to 16.63 mm/day on 7 March 2014, and reached its maximum (59.22 mm/a day) on 8 March, after which it decreased to reach 2.57 mm/day. Furthermore, on 17 January 2010, the area was struck by a storm; its precipitation rate ranged from 0 to 13.45 (mm/day); the precipitation rate ranged from 0 to 9.54 mm/day on 29 December 2010. These seasonal rainfall storms can replenish the shallow aquifers (Figure 4).

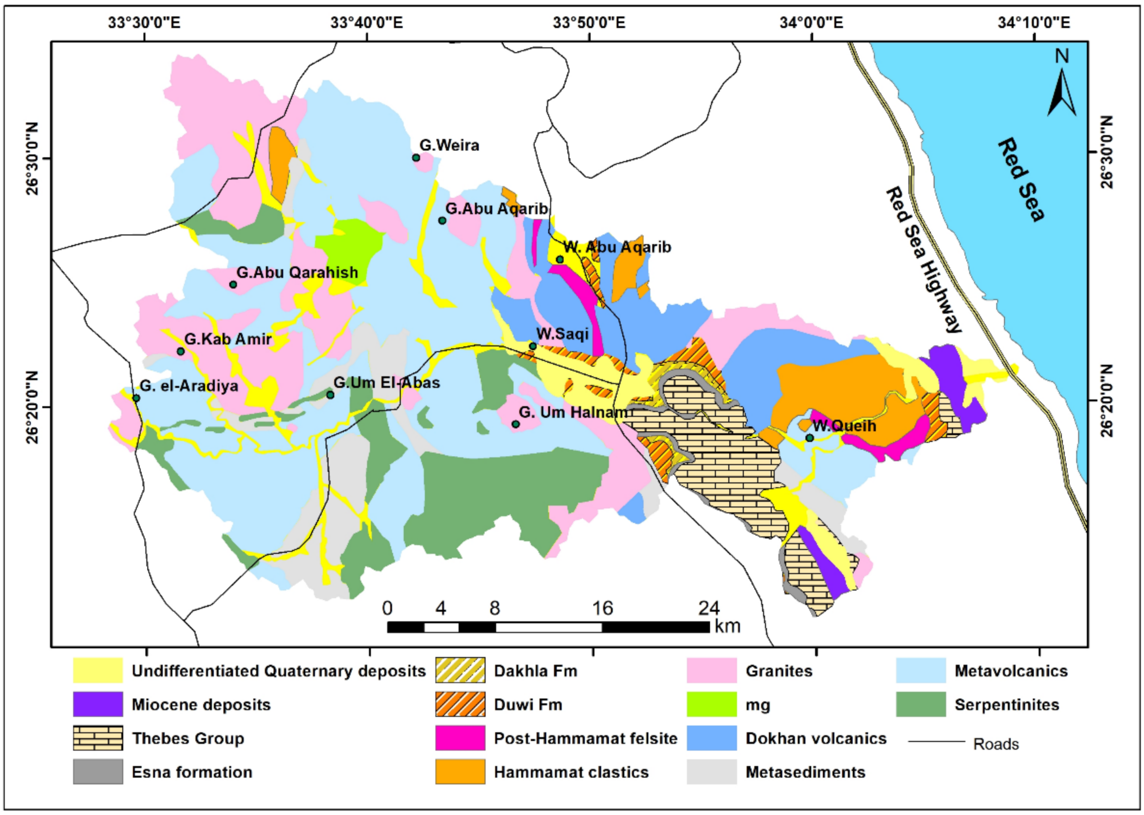

Figure 2. Geological map of the study area.

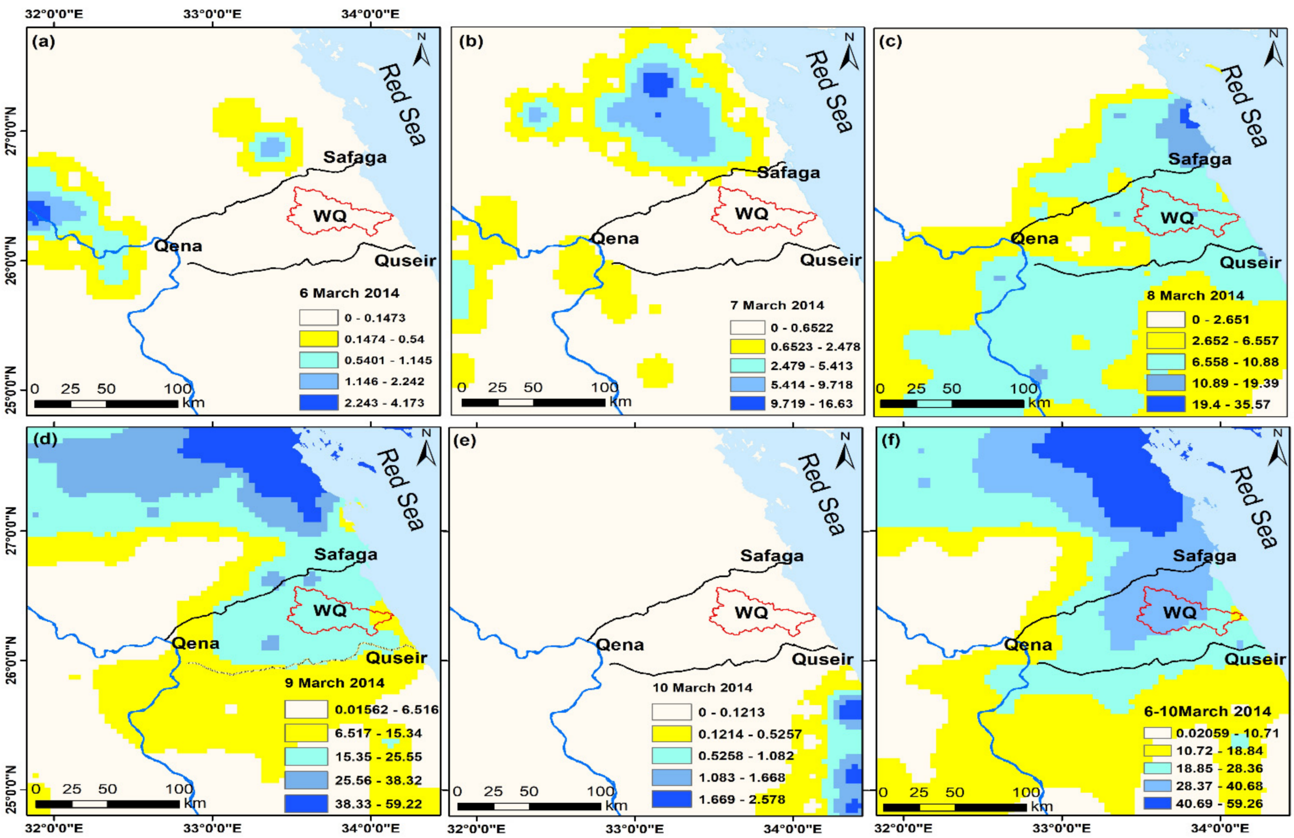

Figure 3. Daily precipitation (mm) on 6 to 10 March 2014, respectively (**a**–**e**), and (**f**) the average covering WQ basin.

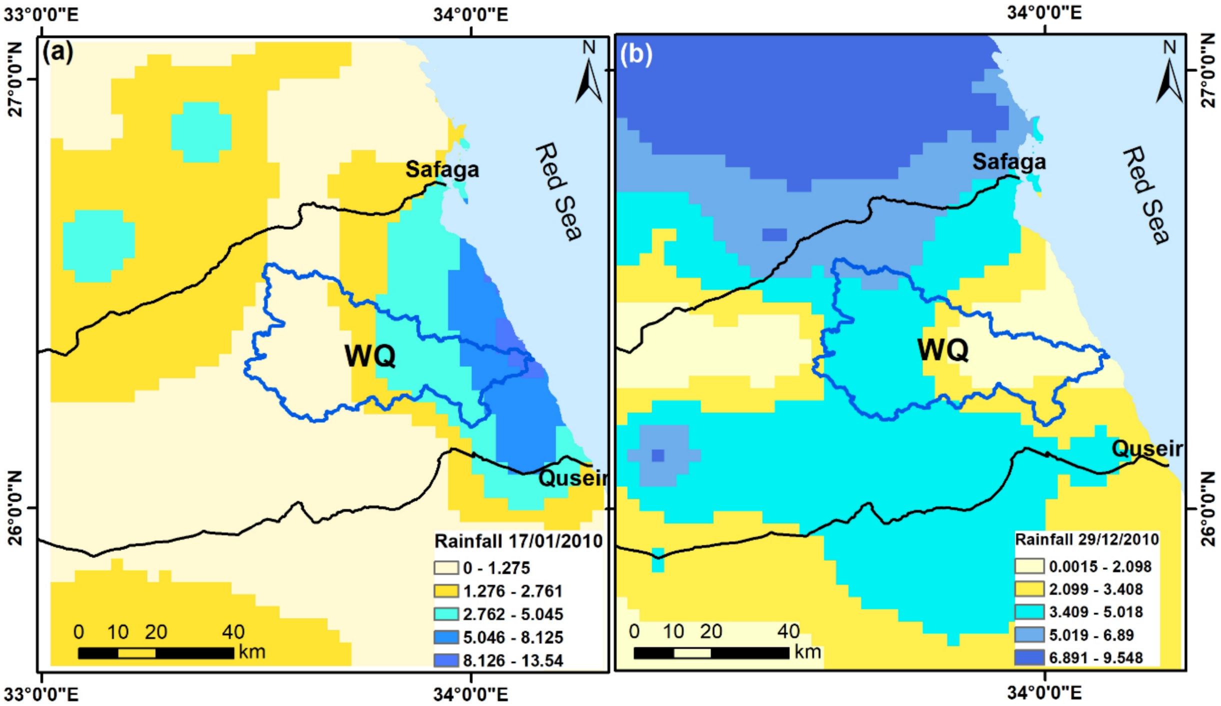

Figure 4. Precipitation rate (mm/day) on 17 January (**a**) and 29 December 2010 (**b**).

3. Data and Methods

Several satellite radar and optical data were collected (Table 1). We selected 13 factors that cover the hydrologic, topographic, geologic, and climatic features. Such factors aid in revealing the optimum areas of rainwater harvesting. Layers representing topographic (elevation, slope, curvature, TRI), hydrologic (Dd, TWI, and DR), climatic (rainfall), ecologic (NDVI, InSAR CCD), and geologic (lineaments, lithology, radar intensity) information were collected with conventional maps to characterize and achieve the goals of the present article through a combination of a GIS technique (Figure 5). The collected data were processed using ENVI, SNAP, and ArcGIS software packages.

Table 1. Collected remote sensing data utilized in the present study.

No.	Type of Data	Source	Date	Resolution
1	Landsat-8 OLI	USGS/NASA	2014 to 2023	bands 2, 3, 4, 5, 6, and 7 (30 m)
2	Sentinel-1	ESA/Copernicus	2014 to 2023	C-band SLC (12.5 m)
3	Sentinel-2	ESA/Copernicus	2014 to 2023	bands 2, 3, 4, 8 ("10" m), 11, and 12 ("20" m)
4	PALSAR-2 JAXA	JAXA	2017	25 m
5	SRTM DEM	USGS	11–22 February 2000	C-band (30 m)
6	TRMM data	NASA	January 1998 to November 2015	0.25 degrees in latitude and longitude

Optical Landsat-8 (OLI) data obtained from 2016 to 2023 showed the changes along the Red Sea and downstream area of WQ. The Landsat-7 ETM archive and Landsat-5 helped us to collect optical images recorded since 1984. Processing Landsat-8 (OLI), images acquired on 30 December 2020, 31 January 2021, 20 March 2021, and 7 May 2021 allowed characterizing the decrease in the collected water in a lake of WQ. OLI data are important for mapping the vegetated areas, which were delineated by applying the visible infrared bands (NDVI = NIR (band 5) − R (band 4) NIR (band 5) + R (band 4)).

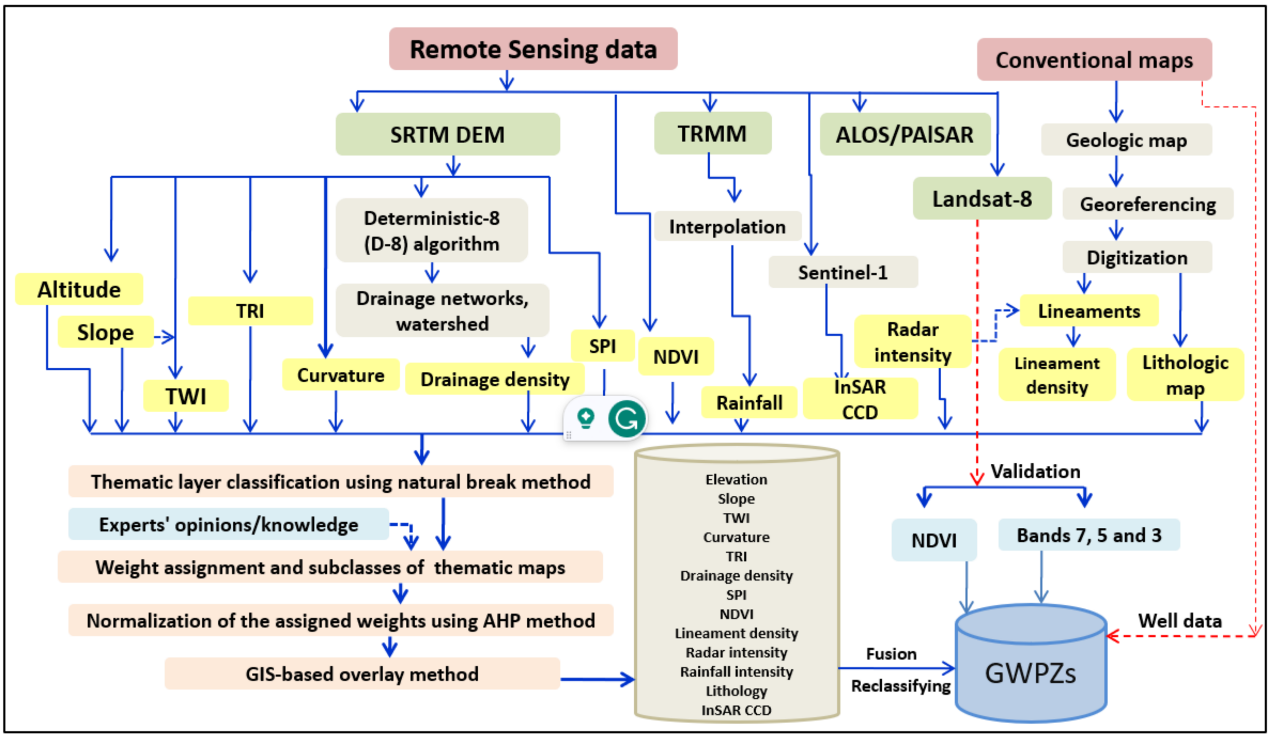

Figure 5. Flowchart representing data and methods utilized in WQ.

In addition to the Landsat series, Sentinel-2 imagery data acquired from 2016 to 2023 were processed to display land use/land cover change detection mapping. Sentinel-2 data come from the ESA spacecraft, an optical satellite platform. This project comprises two land-monitoring satellites covering a wide portion of the Earth's surface, regularly providing high-resolution optical imagery. Sentinel-2 satellites have temporal resolutions of 10 and 5 days, making them extremely valuable for time-series investigations. Two images were acquired on 12 December 2016 and 21 November 22 to display the variation in water resources and vegetation.

Microwave data are effective in hydrologic, geologic, and geomorphic studies and in revealing near-surface features and tectonic movements. SRTM, ALOS/PALSAR, and Sentinel-1 data were collected and implemented to delineate the optimum areas for rainwater harvesting. The interferometric SAR (InSAR) CCD approach can be implemented to assess changes in land cover over time. Using phase and intensity data obtained in SLC-format SAR output, two Sentinel-1 scenes that were collected on 15 August 2019, and 1 March 2021, were combined. This showed modifications to the LUC. The SRTM DEM data (30 m cell size) were implemented to map the topographic characteristics and compute the hydrologic catchments in WQ, Red Sea region. These images were employed widely in mapping surface water runoff and accumulation, revealing the potential areas for harvesting rainwater.

A mosaic of the advanced land observing satellite ALOS and PALSAR-2 satellite provided radar data at different polarization levels using a synthetic aperture radar (SAR) L-band frequency (1257.5 MHz; k 14 22.9 cm) with an incidence angle of 8 to 70 degrees (e.g., HH and HV) was prepared for the entire area. This is a high-tech Japanese land observation satellite with remote-sensing capabilities. PALSAR data are widely used to study and monitor ground surfaces under severe weather conditions. In this investigation, the Jaxa Palsar mosaic (PALSAR-2 Global Forest/Non-forest 2017 Map) characterized by HH polarization at 25 m resolution was applied to emphasize the variance in radar amplitude to reflect soil properties and likely locations of infiltration.

The study area experienced several storms that could replenish groundwater and cause runoff and flood hazards. Therefore, rainfall data collected from the TRMM satellite recordings provided the average rainfall data. The obtained (https://giovanni.gsfc.nasa.gov/giovanni/ accessed on 10 February 2021) average rainfall data were for the period from January 1998 to November 2015. The obtained data include numerous discontinuous storms in December 2010, January 2010, and March 2014 and 2015. Data can be acquired at the Giovanni/NASA website. The precipitation points were interpolated using the Kriging Spatial Analyst method which is an advanced geostatistical procedure that generates an estimated surface from a scattered set of points with z-values.

Each layer was given a weight using the AHP method [59]. A pairwise comparison matrix was then used to compare the prediction layers (Table 2). Each layer's subcategories were given a rank based on how important they were for estimating mineral resources. The main eigenvalue (λ) was determined in this model using the eigenvector technique, and the consistency index (CI) was generated using the formula in Equation (1):

$$\mathrm{CI} = \frac{(\lambda_{\max} - n)}{(n-1)} \tag{1}$$

where n is the number of factors and λ_{max} is the major eigenvalue. The consistency ratio (CR) was produced by using Equation (2). The computed CR was 0 (CR = 0/1.56). The AHP is considered consistent when the CR is <0.1; otherwise, the AHP is insignificant (Table 2).

$$\mathrm{CR} = \frac{\mathrm{CI}}{\mathrm{RCI}} \tag{2}$$

Table 2. Pairwise comparison matrix.

	Elev	Slope	Curvature	TWI	SPI	Rainfall	Lin	Dd	Radar	Litho	NDVI	Coh	TRI	Criteria Weight	λ_{max}
Elev	1.00	0.67	0.67	0.75	1.00	1.20	1.50	0.75	0.86	0.86	0.75	0.86	0.67	0.84	13
Slope	1.50	1.00	1.00	1.13	1.50	1.80	2.25	1.13	1.29	1.29	1.13	1.29	1.00	1.26	13
Curvature	1.50	1.00	1.00	1.13	1.50	1.80	2.25	1.13	1.29	1.29	1.13	1.29	1.00	1.26	13
TWI	1.33	0.89	0.89	1.00	1.33	1.60	2.00	1.00	1.14	1.14	1.00	1.14	0.89	1.12	13
SPI	1.00	0.67	0.67	0.75	1.00	1.20	1.50	0.75	0.86	0.86	0.75	0.86	0.67	0.84	13
Rainfall	0.83	0.56	0.56	0.63	0.83	1.00	1.25	0.63	0.71	0.71	0.63	0.71	0.56	0.70	13
Lin	0.67	0.44	0.44	0.50	0.67	0.80	1.00	0.50	0.57	0.57	0.50	0.57	0.44	0.56	13
Dd	1.33	0.89	0.89	1.00	1.33	1.60	2.00	1.00	1.14	1.14	1.00	1.14	0.89	1.12	13
Radar	1.17	0.78	0.78	0.88	1.17	1.40	1.75	0.88	1.00	1.00	0.88	1.00	0.78	0.98	13
Litho	1.17	0.78	0.78	0.88	1.17	1.40	1.75	0.88	1.00	1.00	0.88	1.00	0.78	0.98	13
NDVI	1.33	0.89	0.89	1.00	1.33	1.60	2.00	1.00	1.14	1.14	1.00	1.14	0.89	1.12	13
Coh	1.17	0.78	0.78	0.88	1.17	1.40	1.75	0.88	1.00	1.00	0.88	1.00	0.78	0.98	13
TRI	1.50	1.00	1.00	1.13	1.50	1.80	2.25	1.13	1.29	1.29	1.13	1.29	1.00	1.26	13

4. Results

The altitude of the area under investigation ranges from 0 to 1040 m (a.s.l), and it has been divided into five zones: 0–247, 248–395, 396–529, 530–654, and 655–1040 m. These zones occupy 8.5, 44.5, 40.7, and 6.3% of the WQ basin (Figure 6a). The low-topography zones are the most favorable areas for water storage [46]. Noteworthily, areas of flat or gentle slopes hold more water than steep slopes; therefore, here, the slope map has been divided into five zones: 0–6.1, 6.1–12, 13–18, 19–26, and 27–67, which cover 34.01, 28.26, 20.39, 12.86, and 4.49, respectively (Figure 6b; Table 3).

Curvature areas that reflect depressions or wadis hold quantities of surface water during rainstorms. The curvature map is divided into four classes: −3,596,632–−105,092.96, −105,092.96–0, 0–116,777.28, and 116,777–2,627,411 (Table 3). They cover 8.5, 44.5, 40.7, and 6.3% of the entire area, respectively (Figure 6c). The TRI is also an important factor in one of the geomorphic factors that are connected to the occurrence of water accumulation. It is classified into four classes: 0.11–0.4, 0.41–0.49, 0.5–0.58, and 0.59–0.89, occupying 15.7, 35.3, 34.3, and 14.7, respectively (Figure 6d).

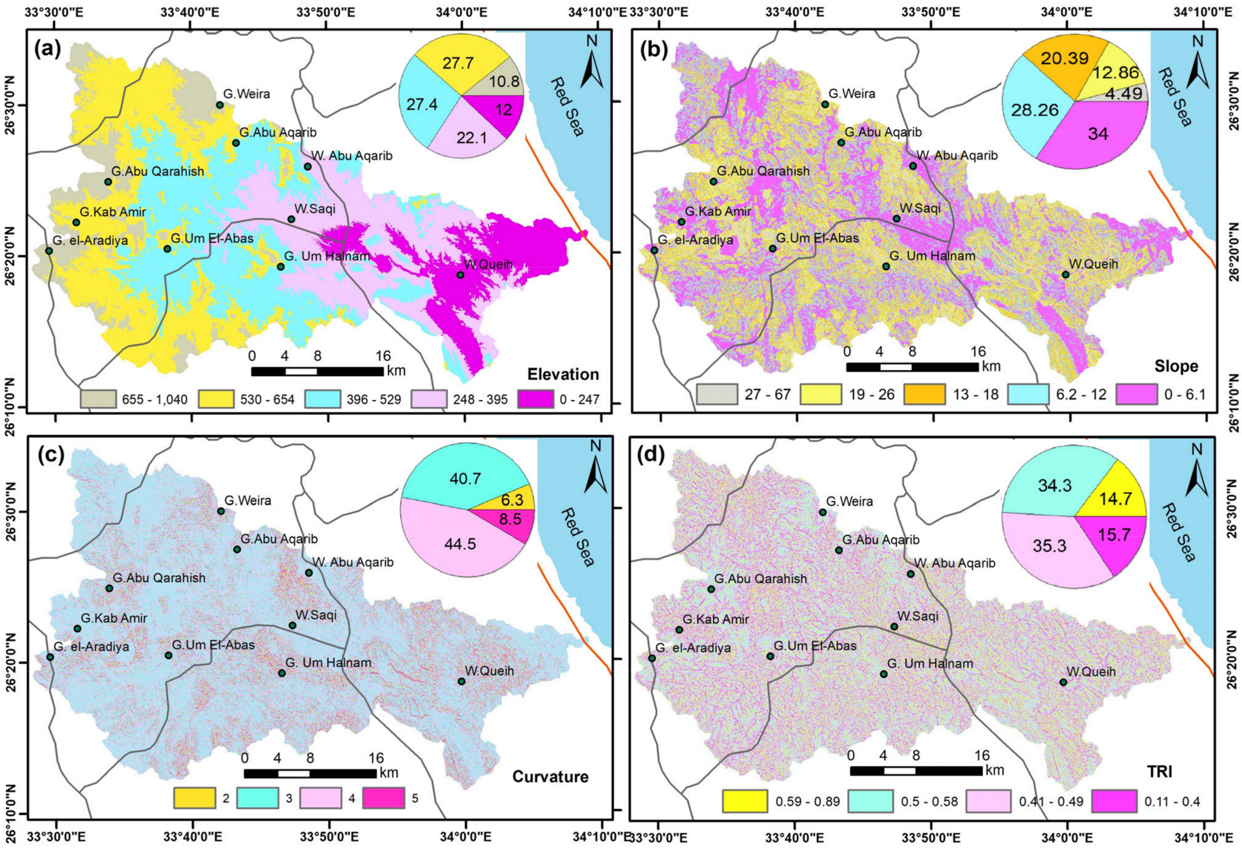

Figure 6. Evidential parameters (**a**) elevation, (**b**) slope, (**c**) curvature, and (**d**) TRI classes of WQ, Red Sea.

Table 3. Factors influencing groundwater occurrence and normalized values.

Elevation	Rank	Normalized Weight %	Area %
0–247	6	0.32	12
248–395	5	0.26	22.1
396–529	4	0.21	27.4
530–654	3	0.16	27.7
655–1039	1	0.05	10.8
Slope			
0–6.1	8	0.286	34.01
6.2–12	7	0.250	28.26
13–18	6	0.214	20.39
19–26	5	0.179	12.86
27–67	2	0.071	4.49
Curvature			
−35 to −10	2	0.143	8.5
−10.1 to 0	3	0.214	44.5
0 to 11	4	0.286	40.7
11 to 26	5	0.357	6.3

Table 3. *Cont.*

Elevation	Rank	Normalized Weight %	Area %
		TRI	
0.11–0.4	5	0.385	15.7
0.41–0.49	4	0.308	35.3
0.50–0.58	3	0.231	34.3
0.59–0.89	1	0.077	14.7
		Dd	
5.2–86	2	0.091	21.9
87–130	5	0.227	30.5
131–179	7	0.318	30.7
180–300	8	0.364	16.9
		TWI	
−8.85 to −4.86	1	0.167	66.8
−4.86–1	2	0.333	30.10
1–13.27	3	0.500	3.10
		SPI	
0–0.25	2	0.20	99.45
0.25–301.27	8	0.80	0.55
		Rainfall	
0.0109–0.0143	2	0.1	19.7
0.0144–0.0167	4	0.2	29.9
0.0168–0.0189	6	0.3	22.8
0.019–0.0213	8	0.4	27.6
		NDVI	
487–949	1	0.056	48.8
949–1367	3	0.167	40.9
1368–1700	6	0.333	8.2
1700–9494	8	0.444	2.1
		Radar	
0–116	5	0.556	42.5
116–193	3	0.333	33.7
193–225	1	0.111	23.8
		Lineaments	
0–17.55	2	0.0952	28.20
17.56–42.70	5	0.2381	30.33
42.71–69.61	6	0.2857	27.41
69.62–149.20	8	0.3810	14.06
		InSAR CCD	
0.08–0.44	7	0.389	8.55
0.44–0.62	6	0.333	20.12
0.62–0.75	3	0.167	35.93
0.75–0.97	2	0.111	35.40

Table 3. *Cont.*

Elevation	Rank	Normalized Weight %	Area %
		Lithology	
Precambrian	2	0.083	3.69
K/T	3	0.125	80.68
Thebes	5	0.208	5.67
Miocene	6	0.250	1.28
Quaternary deposits	8	0.333	8.68

The stream networks were automatically delineated (Figure 7a) and converted into drainage density values (Figure 7b) that are categorized into four classes: 5.2–86, 87–130, 131–179, and 180–300, which cover 16.9, 30.7, 30.5, and 21.9, respectively (Figure 7b). In this basin, areas of high Dd are promising for water occurrence and infiltration. Furthermore, the TWI is one of the crucial terrain factors that are connected to the occurrence of water accumulation. The output of the TWI map was grouped into three classes: low (−8.85 to −4.86), moderate (−4.86 to 1), and high (1 to 13.27), covering about 3.1, 30.1, and 66.8% of the total area, respectively (Figure 7c). Additionally, the stream power index (SPI) was classified into two groups: 0–0.25 and 0.25–301.27, covering 0.55 and 99.45 of the entire area, respectively. The high values correspond to stream areas that received large quantities of water (Figure 7d).

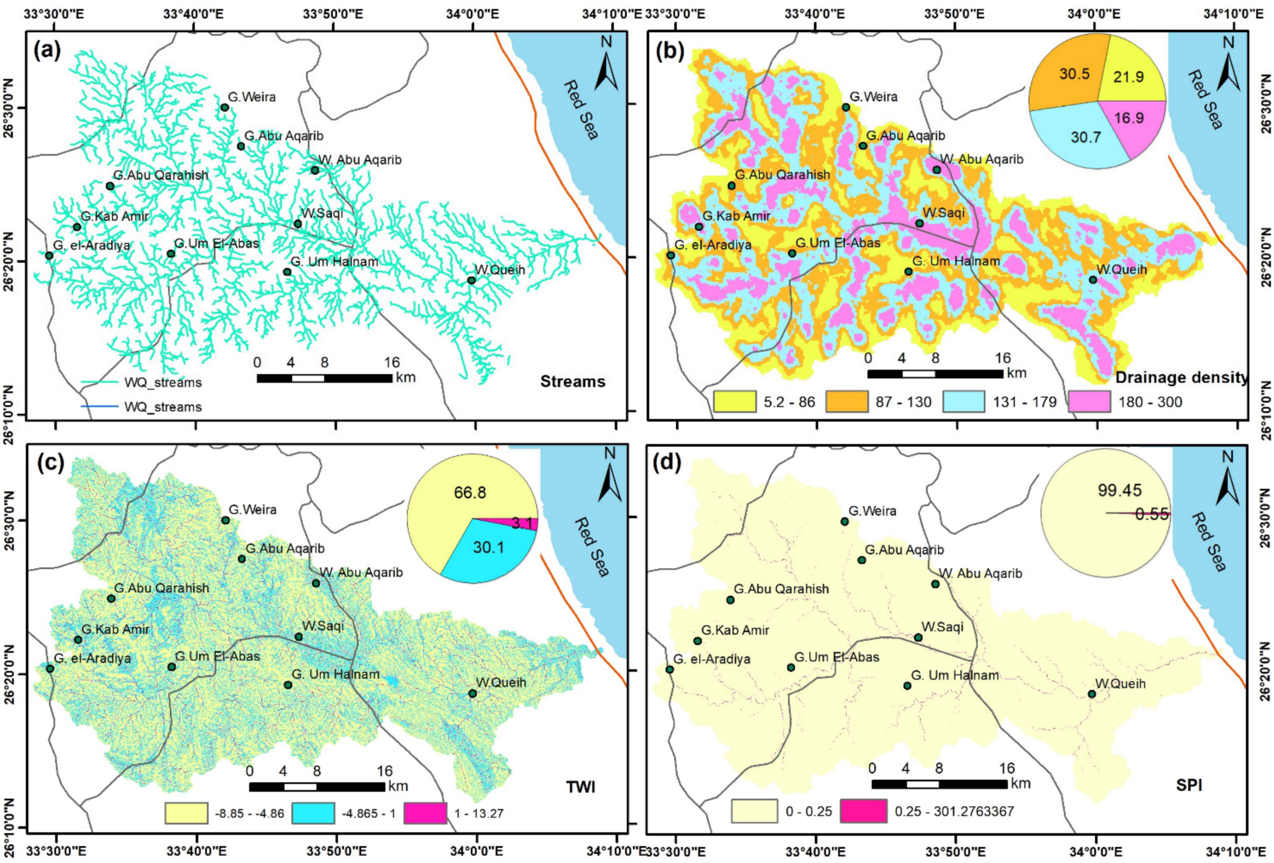

Figure 7. Prospective factors (**a**) stream networks, (**b**) drainage density, (**c**) TWI, and (**d**) SPI classes of Wadi Queih, Red Sea.

Rainfall during rainy storms can promote runoff and water accumulation [7], particularly in areas of low topography (Figure 8a). The rainfall average (mm/day) was obtained for the period from 1 January 1998 to 30 January 2015. Such a map obtained from the TRMM satellite is divided into four classes: 0.109–0.0143, 0.144–0.0167, 0.0168–0.0189, and 0.019–0.0213. These zones cover 19.7, 29.9, 22.8, and 27.6% of the entire area, respectively (Table 3). The vegetated areas allow for lowering the runoff velocity and causing water accumulation. The NDVI layer that was obtained from the Advanced Very High Resolution Radiometer (AVHRR) describes the distribution of the vegetation cover. In general, the NDVI extends from −1 to 1, frequently interpreted as 487 to 9494; a higher NDVI value reflects varied vegetation and healthy plants. The NDVI map is classified into four classes: 487– 949, 949–1367, 1368–1700, and 1700–9494, based on the natural break method, occupying 48.8, 40.9, 2.1, and 8.2% of the entire area, respectively (Figure 8b). Using ALOS/PALSAR-2 satellite data (Figure 8c), the areas of loose sediments are described by low backscatter and, hence, low values. Therefore, the basin is categorized into three groups: low, moderate, and high, occupying 23.8, 33.7, and 42.5% of the total area, respectively (Figure 8c).

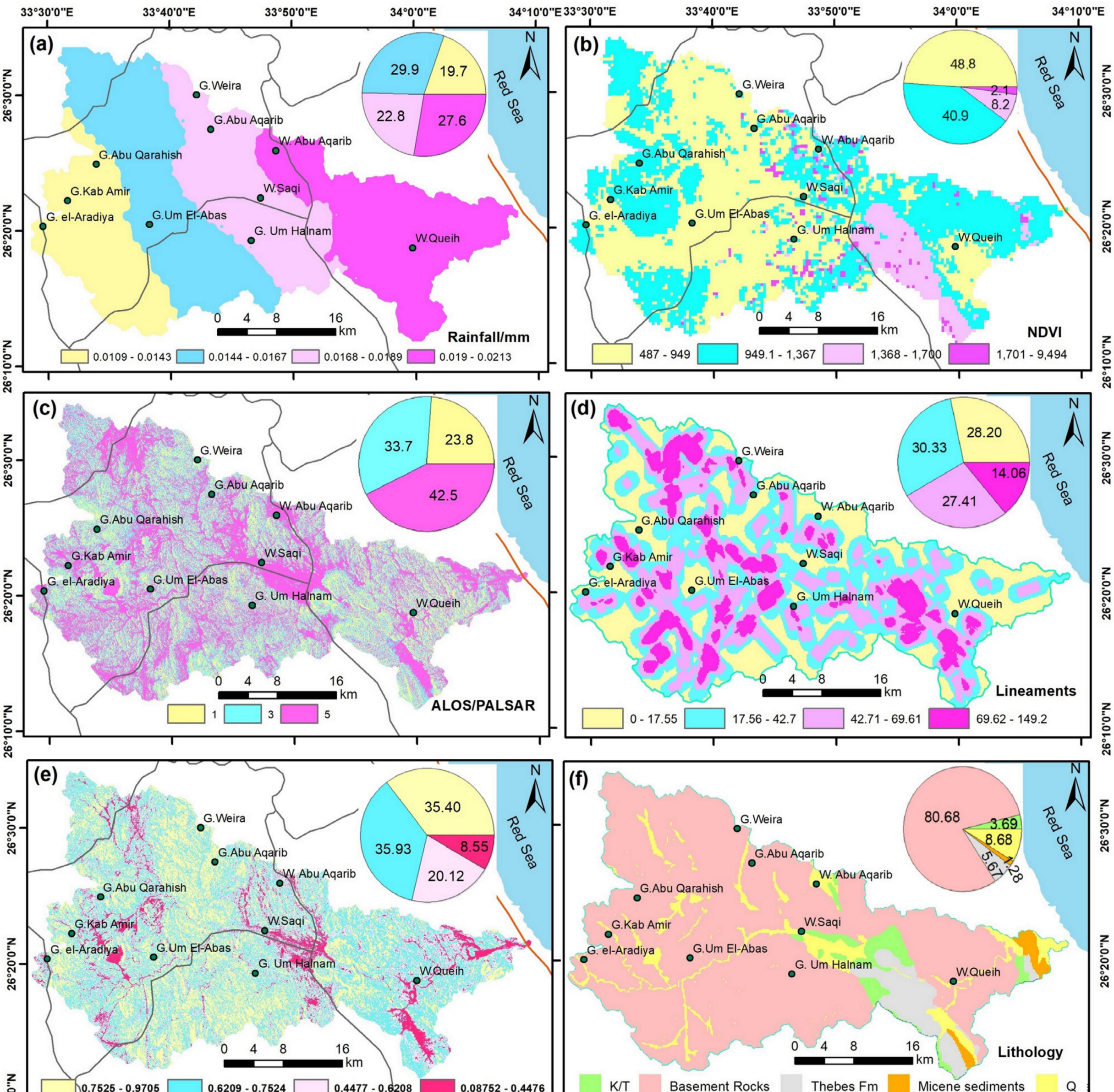

Figure 8. (**a**) Rainfall data acquired from TRMM satellite, (**b**) NDVI, (**c**) ALOS/PALSAR, and (**d**) lineament density classes of WQ, Red Sea; (**e**) InSAR CCD-classified zones; (**f**) simplified geological map.

Lineaments serve as a channel for water movement through strata, which reflects and causes secondary porosity and increases the permeability of the medium [60]. Therefore, the map of lineament density is grouped into four classes: 0–17.55, 17.56–42.7, 42.71–69.61, and 149.2% (Figure 8d). Moreover, the InSAR CCD image (Figure 8e) is classified into four classes; low coherence (0.087–0.447) indicates areas that experienced runoff (Figure 8e). In addition, areas of Quaternary deposits hold groundwater as a result of high infiltration (Figure 8f).

5. Potential Areas of Rainwater Harvesting and Water Accumulation

Based on their respective abilities to hold surface water, the 13 evidentiary maps were merged. Elevation, slope, curvature, TRI, TWI, SPI, drainage density, NDVI, PALSAR, lineaments, InSAR CCD, lithology, and rainfall were the input predictors used to generate the prediction map. The final map was acquired using a multi-criteria GIS-based procedure to overlay the thematic layers, with each cell in a GIS layer fitting to the same pixel region [61]. The resulting map was then categorized into five categories, namely very high, high, moderate, low, and very low potentiality, by integrating 13 thematic maps using the natural break approach (Figure 9). The combination of multiple criteria can be estimated using the following Equation (3):

$$\mathrm{PZWA} = \sum_{i=1}^{n} Li \times Ci \tag{3}$$

where Li refers to the normalized grade of evidence of the i factor and Ci is connected to the rank of the sub-classes.

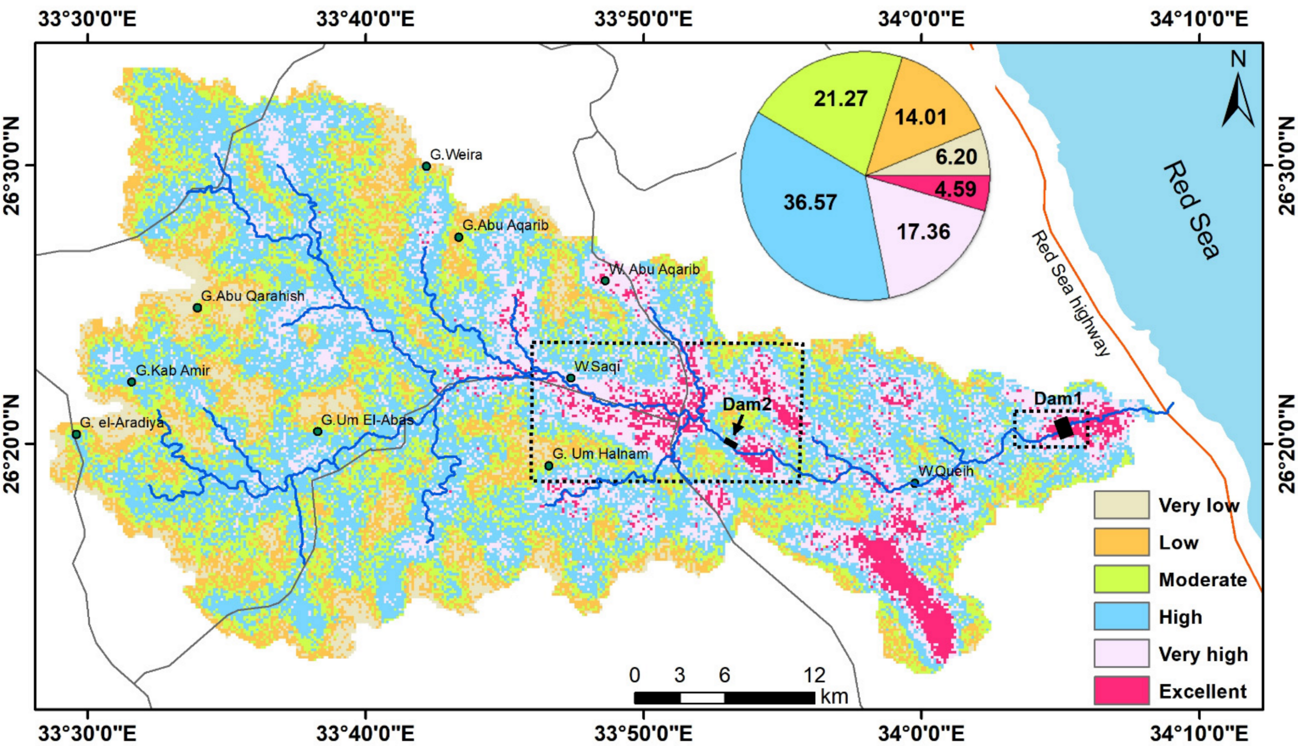

Figure 9. Potential areas of water accumulation in WQ. The dot frame is magnified and displayed in Figure 12.

Rainwater is permitted to flow from the top reaches and is collected for continued crop and plant growth in the lower reaches [13]. Two areas were suggested for harvesting rainfall and initiating artificial lakes and dams; one of these areas is the downstream area of WQ (Figure 9), and the second area is at the intersection of W. Saqi and W. Abu Aqarib, where a low-topography area occurs between basement rocks and Cretaceous/Tertiary rocks. This is a significant use for reclaiming water for agriculture in the case of climate change and increasing rainfall. The dam site is a drainage point situated at the downstream-most point in the catchment. The best dam site for storage was suggested based on the short length, high water storage volume, and low cost. A dam has been built in the WQ basin to effectively utilize rainwater, particularly along the narrow stretches of the basin's mild slope courses. These considerations include dams that slow down and contain moving water. Furthermore, dams sometimes referred to as flood retention or multipurpose dams ought to be built so that flood courses follow a zigzag pattern. An arrangement like this will help to ensure that floodwater is used as efficiently as possible, prevent severe flash floods and soil erosion, maximize and promote groundwater recharge, raise the water level in the wells below the dam to make up for the excessive lack of farmers in the area, and stop running water from entering the Red Sea [62,63].

The InSAR CCD image (Figure 10a) displays the range from 0 to 0.97, the highly changing characteristics at extremely low cohesiveness values close to 0 (rapid change), and the regions at high coherence values close to 1. The low SAR coherence values can be utilized to identify anthropogenic or natural changes in vegetation or water. The vegetation that grows downstream of WQ is depicted in green on the Landsat 8 band composite 7, 5, and 3 (2016, 2022), while the gathered water below the dam is shown in a darker hue (January 2021) in the Sentinel-2 and high-resolution Google Earth image (Figure 10 b–d). The gathered water is vital to sustaining urban and agricultural expansion. A portion of the topmost water that was trapped would have seeped into the soil and refilled the permeable wadi deposits during the rainy season. Substantial aggregates of freshwater may have seeped into the subterranean porous deposits, making these locations highly promising for groundwater accretion and deserving of additional geoelectric investigation.

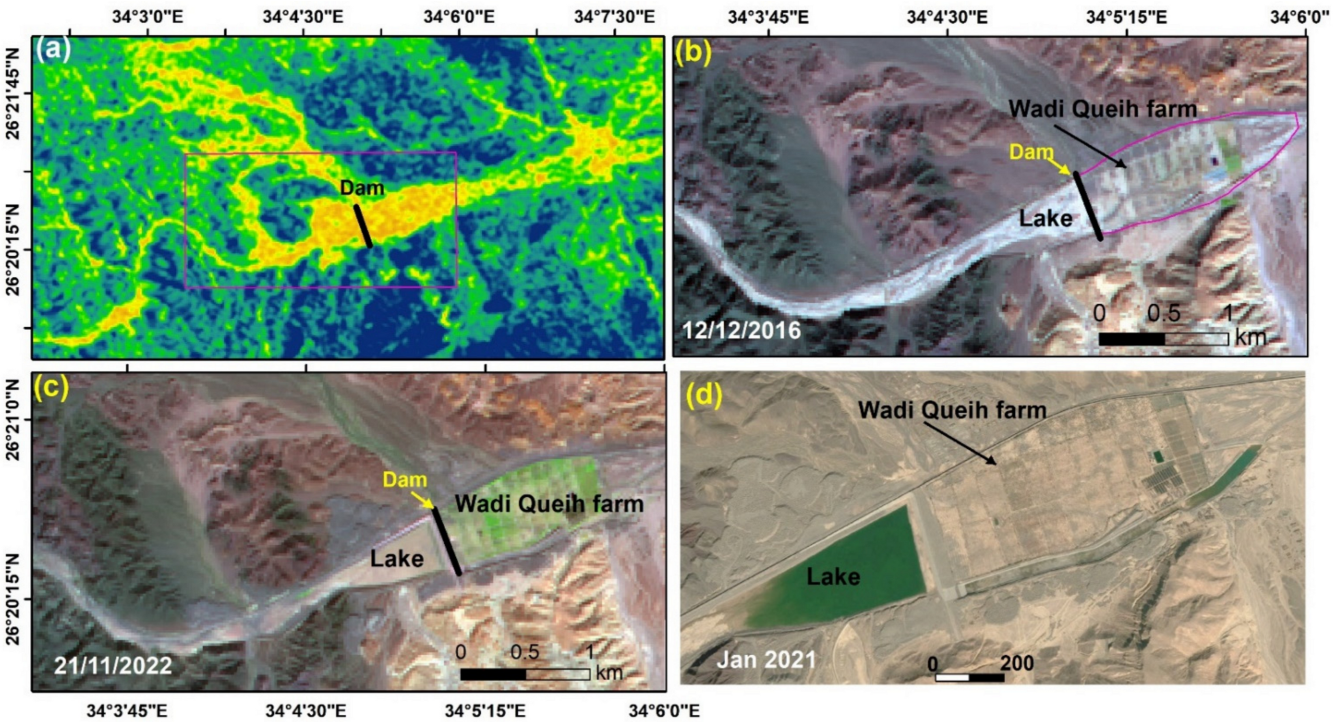

Figure 10. (**a**) InSAR CCD of VH of the downstream area revealing changes in land use/cover between 15 August 2019 and 01 March 2021; the portion of the image enclosed by the purple box has been magnified and is indicated in (**b**,**c**). (**b**) Promising areas of water accumulation, including the erected dam at WQ farm and (**c**,**d**) the proposed area for erecting a dam and lake at the intersection of Wadi Abu Aqarib, W. Um Halnam, and Wadi Saqi.

The primary captured flood water is reached via the flood canal, which collects water and directs it to irrigate a farm. This watercourse was built to manage runoff and overflow from the rain. The down-dam's newly constructed canal is intended to quickly drain rainwater during rains. Holding dams are used to hold excess water so that they can benefit plant reclamation areas, replenish groundwater aquifers, or safeguard beaches and marine ecosystems. Given the high rate of evaporation in the region, it is advised to make lakes deeper and with a smaller surface area to limit water loss through evaporation. A suitable layout of the dam's water outflow is carefully planned to securely release any water to irrigate crops (Figure 10c,d).

6. Discussion

Climate change has resulted in an increase in rainstorms as well as an increase in the possibility of disasters because of runoff and flash flooding [46,47]. Therefore, catching such water resources becomes an important issue in converting water scarcity into abundance [9,24,25,38,47,64]. Such water supplies captured from rainwater can be utilized for sustainable development and supporting settlements in the downstream areas (Figures 11 and 12). This would allow for land reclamation in the downstream areas based on the amount of water. Moreover, catching water and controlling rainwater discharge protect marine ecosystems, especially coral reefs, from contaminants and excessive sediments resulting from flash floods. Therefore, understanding the topographic, hydrologic, and lithologic characteristics of the catchments is significant for revealing the optimum areas for rainwater harvesting.

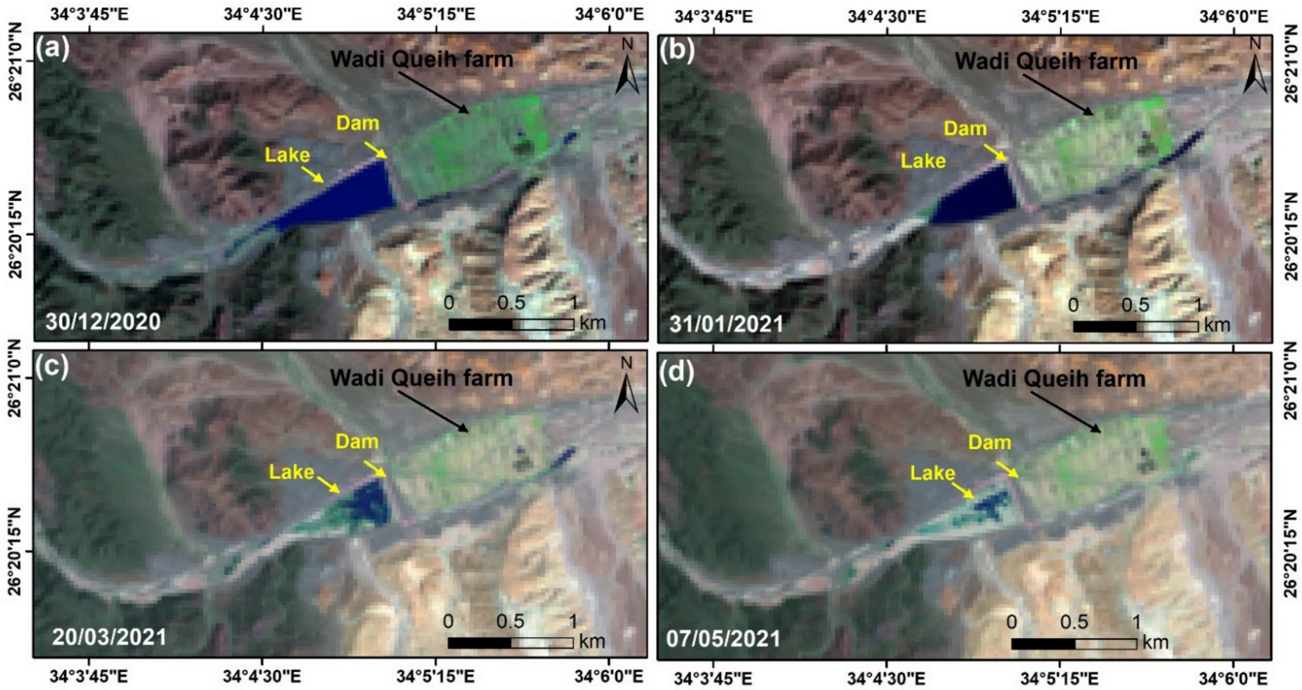

Figure 11. (**a**–**d**) Landsat series obtained after a storm in December 2020, revealing the existence of water behind a dam in WQ.

Several factors that have the capability of influencing the harvesting of rainfall water resources are rainfall intensity and seasonal storms, topographic characteristics, soil conditions, the characteristics of the catchment area, and land use and land cover. Less RWH potential exists in steeper slope areas because they increase runoff velocity and reduce channel capacity for holding water [47,65] in the upper stream areas (Figure 13). Additionally, drainage density, which is connected to infiltration capacity, climate, and erosion resistance [17,66], has a favorable relationship with RWH potentiality [65]. Areas of sand and lineament density would hold groundwater resources. Because of secondary as well as primary porosity, a significant amount of water would have been recharged into the rocks beneath the sands [12,34]. Therefore, regions that included significant sand collections in the chosen study area could have enormous resources of groundwater [26,41], like the vicinity of the point of intersection between W. Abu Aqarib, W. Saqi, and W. Um Halnam. After rainstorms, the accumulated water can evaporate and appear in white tones in satellite images. The white spots in Landsat images are salt evaporation; they are extremely bright spots left over from evaporated lake water and are indicative of surface water buildup (Figure 10b). These white spots show salt concentration in the type of salt layers that cover and fill the surface sediments [67].

The erected dam at the downstream area allowed for holding approximately 1 million m^3 of rainwater after rainy storms based on the measured lake capacity (Figure 11). The planners utilized such water in planting the WQ farm; part of such water can be evaporated, and the rest would recharge the groundwater aquifer, as indicated by the gradual decrease in surface water areas from December 2020 to May 2021 (Figure 11). The dam helps secure water supplies to irrigate the farm and other industrial activities in the area. Despite the fact that the model appears to be effective at a reasonable level, the expected results are affected by the resolution and amount of utilized input information and images, as well as the field validation. Regarding future works, the integration of multiple criteria through analysis using RS and GIS techniques is recommended for applications in other areas with different environmental conditions.

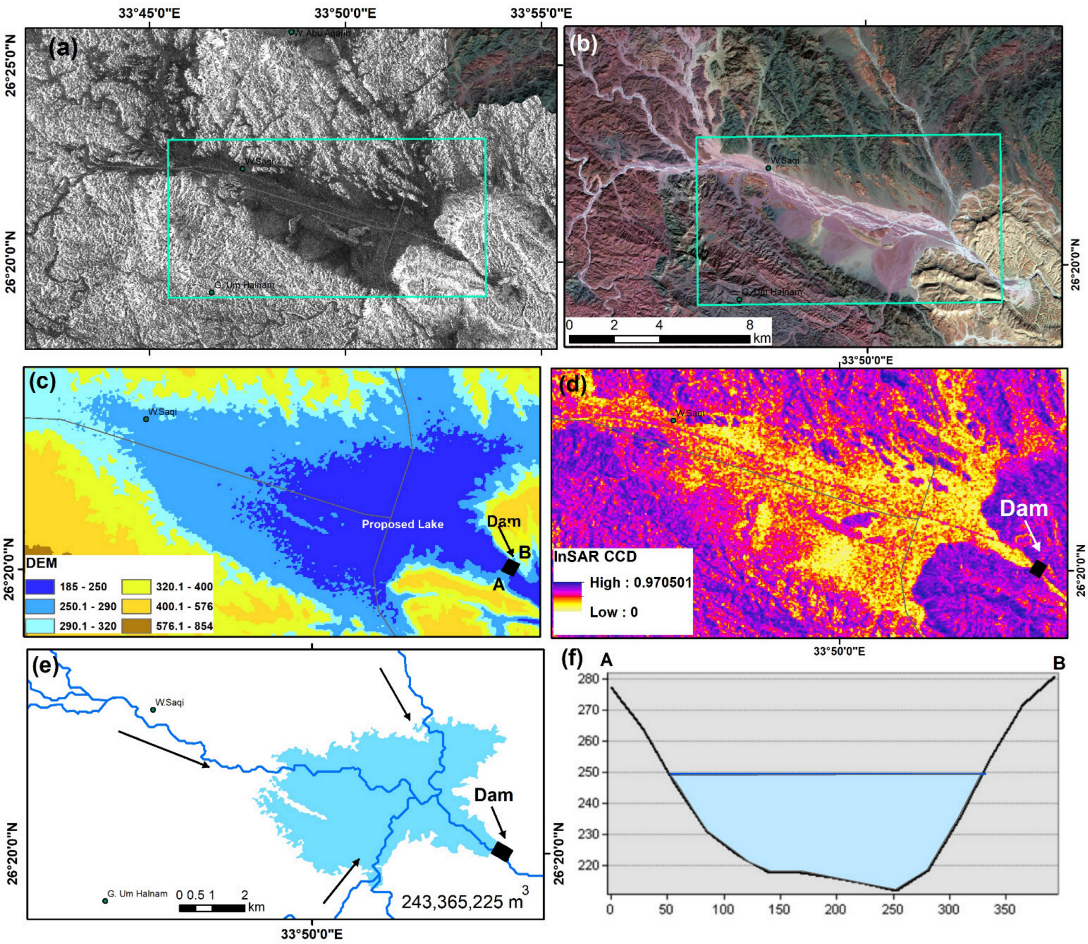

Figure 12. (**a**) ALOS/PALSAR image of the selected area at W. Saqi; (**b**) Landsat OLI 7, 5 and 3 in R, G, and B; (**c**) a DEM of the area as appears in (**a**); (**d**) InSAR CCD of the area VH_15Aug2019_01Mar2021; (**e**) proposed lake area; (**f**) A-B cross-section through the suggested lake, representing AB indicated in (**c**). The cyan polygon in (**a**,**b**) is magnified and displayed in (**c**–**e**).

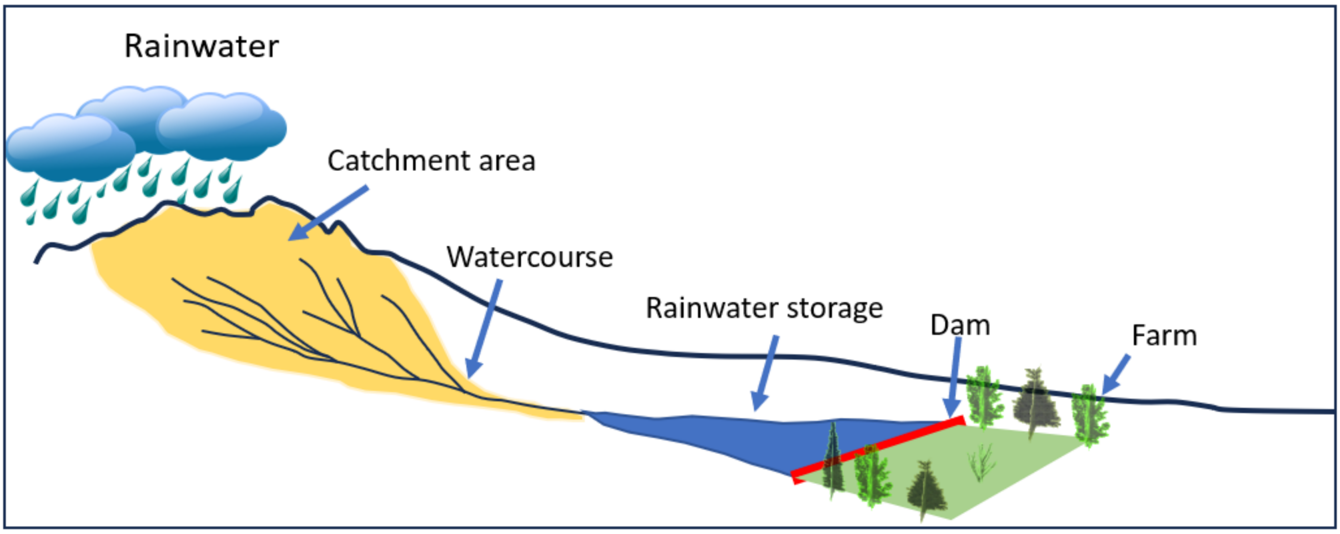

Figure 13. Rainwater harvesting model adopted in the present study and water accumulation during rainstorms.

7. Conclusions

Harvesting water resources is a significant issue in sustainable development. In this project, multiple criteria derived from remote sensing, geologic, climatic, and hydrologic data were combined to reveal a promising area for RWH and water accumulation. The 13 evidential layers, namely elevation, slope, TWI, SPI, TRI, curvature, Dd, radar intensity, distance to the river, InSAR CCD, NDVI, lithology, and rainfall, were initiated and merged to reveal promising areas for water accumulation. The resulting map is categorized into six distinguishing classes, dependent on their potential for groundwater: very low (6.20%), low (14.01%), moderate (21.26%), high (36.57%), very high (17.35%), and excellent areas (4.59%). It is recommended to erect a dam at the joining of W. Abu Aqarib, W. Saqi, and W. Um Halnam that can capture about 240 million m^3. InSAR CCD revealed that the areas of no coherence are consistent with very-high to excellent zones. In summary, the study proved that the utilized GIS and remote sensing techniques are trustworthy and affordable and may be used to locate potential locations for harvesting rainfall and assist planners and decision-makers.

Author Contributions: Conceptualization, M.A.; methodology, M.A.; software, M.A.; validation, M.A.; investigation, M.A.; resources, M.A. and A.M.M.; writing—original draft preparation, M.A., A.M.M. and A.A.; writing—review and editing, M.A., A.M.M. and A.A. All authors have read and agreed to the published version of the manuscript.

Funding: This research was funded by the Academy of Scientific Research and Technology (ASRT), grant number 19476. The APC was funded by ASRT.

Data Availability Statement: Not applicable.

Conflicts of Interest: The authors declare no conflict of interest.

Abbreviations

SRTM	Shuttle Radar Topography Mission	DEM	Digital Elevation Model
TRMM	Tropical Rainfall Measuring Mission	OLI	Operational Land Imager
ALOS	Advanced Land Observing Satellite	RS	Remote Sensing
PALSAR	Phased-Array-Type L-band Synthetic Aperture Radar	AHP	Analytical Hierarchy Process
GIS	Geographic Information System	LU/LC	Land Use/Land Cover
TWI	Topographic Wetness Index	NIR	Near Infrared

PZWA	Prospective Zones of Water Accumulation	SNAP	The Sentinel Application Platform
InSAR	Interferometry Synthetic Aperture Radar	CCD	Coherence Change Detection
NDVI	Normalized Difference Vegetation Index	MHz	Megahertz
8D	Deterministic Eight-Neighbors	CR	Consistency Ratio
USGS	United States Geological Survey	CI	Consistency Index
TRI	Terrain Roughness Index	SLC	Single Look Complex
ENVI	Environment for Visualizing Images	R	Red Band
WGS 84	World Geodetic System 1984	DR	Distance to River
Dd	Drainage Density	Lin	Lineaments
Lith	Lithology	Rad	Radar Intensity
Curv	Curvature	GW	Groundwater
NE	Northeast	SW	Southwest

References

1. FAO. *Coping with Water Scarcity: An Action Framework for Agriculture and Food Security*; Food and Agriculture Organization of the United Nations: Rome, Italy, 2012; p. 100.
2. FAO. *Climate Change and Food Security: Risks and Responses*; Food and Agriculture Organization of the United Nations: Rome, Italy, 2015; p. 122.
3. FAO. *Towards a Water and Food Secure Future: Critical Perspectives for Policy-Makers*; Food and Agriculture Organization of the United Nations: Rome, Italy, 2015; p. 61. Available online: http://www.fao.org/nr/water/docs/FAO_WWC_white_paper_web.pdf (accessed on 12 March 2023).
4. IPCC. *Climate Change: Synthesis Report. Contribution of Working Groups I, II, and III to the Fifth Assessment Report of the Intergovernmental Panel on Climate Change*; Core Writing Team, Pachauri, R.K., Meyer, L.A., Eds.; IPCC: Geneva, Switzerland, 2014; p. 151.
5. IPCC. Sections. In *Climate Change 2023: Synthesis Report. Contribution of Working Groups I, II and III to the Sixth Assessment Report of the Intergovernmental Panel on Climate Change*; Core Writing Team, Lee, H., Romero, J., Eds.; IPCC: Geneva, Switzerland, 2023; pp. 35–115. [CrossRef]
6. Furumai, H. Rainwater and reclaimed wastewater for sustainable urban water use. *Phys. Chem. Earth Parts A/B/C* **2008**, *33*, 340–346. [CrossRef]
7. Guo, Z.; Torra, O.; Hürlimann, M.; Abancó, C.; Medina, V. FSLAM: A QGIS plugin for fast regional susceptibility assessment of rainfall-induced landslides. *Environ. Model. Softw.* **2022**, *150*, 105354. [CrossRef]
8. Ffolliott, P.F.; Brooks, K.N.; Neary, D.G. Water harvesting in arid and semi-arid regions. *Hydrol. Water Resour. Ariz. Southwest J.* **2014**, *43*, 41–44. Available online: http://hdl.handle.net/10150/627369 (accessed on 10 May 2023).
9. Zheng, H.; Gao, J.; Xie, G.; Jin, Y.; Zhang, B. Identifying important ecological areas for potential rainwater harvesting in the semi-arid area of Chifeng, China. *PLoS ONE* **2018**, *13*, e0201132. [CrossRef]
10. UNEP. *Rainwater Harvesting and Utilization: An Environmentally Sound Approach for Sustainable Urban Water Management: An Introductory Guide for Decision-Makers*; UNEP: Osaka, Japan, 2002; Available online: https://www.ircwash.org/sites/default/files/213.1-01RA-17421.pdf (accessed on 10 May 2023).
11. UN-HABITAT. *Rainwater Harvesting and Utilization*; UN-HABITAT: Nairobi, Kenya, 2005; Available online: https://sswm.info/sites/default/files/reference_attachments/UN-HABITAT%202005%20Rainwater%20Harvesting%20and%20Utilisation%20Book%202.pdf (accessed on 8 July 2023).
12. Razandi, Y.; Pourghasemi, H.R.; Neisani, N.S.; Rahmati, O. Application of analytical hierarchy process, frequency ratio, and certainty factor models for groundwater potential mapping using GIS. *Earth Sci. Inform.* **2015**, *8*, 867–883. [CrossRef]
13. Alarifi, S.S.; Abdelkareem, M.; Abdalla, F.; Alotaibi, M. Flash Flood Hazard Mapping Using Remote Sensing and GIS Techniques in Southwestern Saudi Arabia. *Sustainability* **2022**, *14*, 14145. [CrossRef]
14. Abdel-Shafy, H.I.; El-Sahary, A.A.; Regelsberger, M.; Platzer, C. Rainwater in Egypt: Quantity, distribution, and harvesting. *Mediterr. Mar. Sci.* **2010**, *11*, 245–257. [CrossRef]
15. Manap, M.A.; Sulaiman, W.N.A.; Ramli, M.F.; Pradhan, B.; Surip, N. A knowledge-driven GIS modeling technique for groundwater potential mapping at the Upper Langat Basin, Malaysia. *Arab. J. Geosci.* **2011**, *6*, 1621–1637. [CrossRef]
16. Avand, M.; Janizadeh, S.; Tien Bui, D.; Pham, V.H.; Ngo, P.T.T.; Nhu, V.-H. A tree-based intelligence ensemble approach for spatial prediction of potential groundwater. *Int. J. Digit. Earth* **2020**, *13*, 1408–1429. [CrossRef]
17. Abdelkareem, M.; Abdalla, F. Revealing potential areas of water resources using integrated remote-sensing data and GIS-based analytical hierarchy process. *Geocarto Int.* **2022**, *37*, 8672–8696. [CrossRef]
18. Zhu, Q.; Abdelkareem, M. Mapping groundwater potential zones using a knowledge-driven approach and GIS analysis. *Water* **2021**, *13*, 579. [CrossRef]
19. Wheater, H.S.; Mathias, S.A.; Li, X. *Groundwater Modelling in Arid and Semi-Arid Areas*; Cambridge University Press: Cambridge, UK, 2010; pp. 119–130.
20. Rahman, A. A GIS-based DRASTIC model for assessing groundwater vulnerability in shallow aquifer in Aligarh, India. *Appl. Geogr.* **2008**, *28*, 32–53. [CrossRef]

21. Mondal, N.C.; Adike, S.; Singh, V.S.; Ahmed, S.; Jayakumar, K.V. Determining shallow aquifer vulnerability by the DRASTIC model and hydrochemistry in granitic terrain, southern India. *J. Earth Syst. Sci.* **2017**, *126*, 89. [CrossRef]
22. Mondal, N.C.; Adike, S.; Ahmed, S. Development of entropy-based model for pollution risk assessment of hydrogeological system. *Arab. J. Geosci.* **2018**, *11*, 375. [CrossRef]
23. Yeh, H.-F.; Cheng, Y.-S.; Lin, H.-I.; Lee, C.-H. Mapping groundwater recharge potential zone using a GIS approach in Hualian River, Taiwan. *Sustain. Environ. Res.* **2016**, *26*, 33–34. [CrossRef]
24. De Winnaar, G.; Jewitt, G.P.W.; Horan, M. A GIS-based approach for identifying potential runoff harvesting sites in the Thukela River basin, South Africa. *Phys. Chem. Earth* **2007**, *32*, 1058–1067. [CrossRef]
25. Mahmoud, S.H.; Alazba, A.A. The potential of in situ rainwater harvesting in arid regions: Developing a methodology to identify suitable areas using GIS-based decision support system. *Arab. J. Geosci.* **2014**, *8*, 5167–5179. [CrossRef]
26. Rejani, R.; Rao, K.V.; Srinivasa Rao, C.H.; Osmano, M.; Sammi Reddy, K.; George, B.; Pratyusha Kranthi, G.S.; Chary, G.R.; Swamy, M.V.; Rao, P.J. Identification of potential rainwater-harvesting sites for the sustainable management of a semi-arid watershed. *Irrig. Drain.* **2017**, *66*, 227–237. [CrossRef]
27. Li, Y.; Abdelkareem, M.; Al-Arifi, N. Mapping Potential Water Resource Areas Using GIS-Based Frequency Ratio and Evidential Belief Function. *Water* **2023**, *15*, 480. [CrossRef]
28. Machiwal, D.; Rangi, N.; Sharma, A. Integrated knowledge- and data-driven approaches for groundwater potential zoning using GIS and multi-criteria decision-making techniques on hard-rock terrain of Ahar catchment, Rajasthan, India. *Environ. Earth Sci.* **2014**, *73*, 1871–1892. [CrossRef]
29. Rahmati, O.; Samani, A.N.; Mahdavi, M.; Pourghasemi, H.R.; Zeinivand, H. Groundwater potential mapping at Kurdistan region of Iran using analytic hierarchy process and GIS. *Arab. J. Geosci.* **2014**, *8*, 7059–7071. [CrossRef]
30. Kumar, V.A.; Mondal, N.C.; Ahmed, S. Identification of Groundwater Potential Zones Using RS, GIS and AHP Techniques: A Case Study in a Part of Deccan Volcanic Province (DVP), Maharashtra, India. *J. Indian Soc. Remote Sens.* **2020**, *48*, 497–511. [CrossRef]
31. Riad, P.; Billib, M.; Hassan, A.; Salam, M.A.; El Din, M.N. Application of the overlay weighted model and boolean logic to determine the best locations for artificial recharge of groundwater. *J. Urban Environ. Eng.* **2011**, *5*, 57–66. [CrossRef]
32. Mallick, J.; Khan, R.A.; Ahmed, M.; Alqadhi, S.D.; Alsubih, M.; Falqi, I.; Hasan, M.A. Modeling Groundwater Potential Zone in a Semi-Arid Region of Aseer Using Fuzzy-AHP and Geoinformation Techniques. *Water* **2019**, *11*, 2656. [CrossRef]
33. Sun, T.; Cheng, W.; Abdelkareem, M.; Al-Arifi, N. Mapping Prospective Areas of Water Resources and Monitoring Land Use/Land Cover Changes in an Arid Region Using Remote Sensing and GIS Techniques. *Water* **2022**, *14*, 2435. [CrossRef]
34. Abdekareem, M.; Al-Arifi, N.; Abdalla, F.; Mansour, A.; El-Baz, F. Fusion of Remote Sensing Data Using GIS-Based AHP-Weighted Overlay Techniques for Groundwater Sustainability in Arid Regions. *Sustainability* **2022**, *14*, 7871. [CrossRef]
35. Adham, A.; Riksen, M.; Ouessar, M.; Ritsema, C. Identification of suitable sites for rainwater harvesting structures in arid and semi-arid regions: A review. *Int. Soil Water Conserv. Res.* **2016**, *4*, 108–120.
36. Ajaykumar, K.K.; Sanjay, S.K.; Nagesh, N.P.; Pawar, N.J.; Sankhua, R.N. Identifying Potential Rainwater Harvesting Sites of a Semi-arid, Basaltic Region of Western India, Using SCS-CN Method. *Water Resour Manag.* **2012**, *26*, 2537–2554.
37. Hürlimann, M.; Guo, Z.; Puig-Polo, C.; Medina, V. Impacts of future climate and land cover changes on landslide susceptibility: Regional scale modeling in the Val d'Aran region (Pyrenees, Spain). *Landslides* **2022**, *19*, 99–118. [CrossRef]
38. Hong, Y.; Abdelkareem, M. Integration of remote sensing and a GIS-based method for revealing prone areas to flood hazards and predicting optimum areas of groundwater resources. *Arab. J. Geosci.* **2022**, *15*, 114. [CrossRef]
39. Chenini, I.; Ben Mammou, A. Groundwater recharge study in arid region: An approach using GIS techniques and numerical modeling. *Comput. Geosci.* **2010**, *36*, 801–817. [CrossRef]
40. Deepa, S.; Venkateswaran, S.; Ayyandurai, R.; Kannan, R.; Vijay Prabhu, M. Groundwater recharge potential zones mapping in upper Manimuktha Sub-basin Vellar river Tamil Nadu India using GIS and remote sensing techniques. *Model. Earth Syst. Environ.* **2016**, *2*, 137. [CrossRef]
41. Abdelkareem, M.; El-Baz, F. Analyses of optical images and radar data reveal structural features and predict groundwater accumulations in the central Eastern Desert of Egypt. *Arab. J. Geosci.* **2015**, *8*, 2653–2666. [CrossRef]
42. Chowdhury, A.; Jha, M.K.; Chowdhury, V.M.; Mal, B.C. Integrated remote sensing and GIS-based approach for assessing groundwater potential in West Mednapur district, West Bengal, India. *Int. J. Remote Sens.* **2009**, *30*, 231–250. [CrossRef]
43. Abdelkareem, M.; El-Baz, F.; Askalany, M.; Akawy, A.; Ghoneim, E. Groundwater prospect map of Egypt's Qena Valley using data fusion. *Int. J. Image Data Fusion* **2012**, *3*, 169–189. [CrossRef]
44. Satapathy, I.; Syed, T.H. Characterization of groundwater potential and artificial recharge sites in Bokaro District, Jharkhand (India), using remote sensing and GIS-based techniques. *Environ. Earth Sci.* **2015**, *74*, 4215–4232. [CrossRef]
45. Sonbol, M.A. Sustainable Systems of Water Harvesting in Arid Regions, A Case Study: Sinai Peninsula–Egypt. In Proceedings of the 2nd International Conference on Water Resources & Arid Environment, Riyadh, Saudi Arabia, 26–29 November 2006; pp. 1–13.
46. Abdelkareem, M. Targeting flash flood potential areas using remotely sensed data and GIS techniques. *Nat. Hazards J.* **2017**, *85*, 19–37. [CrossRef]
47. Abdelkareem, M.; Mansour, A. Risk assessment and management of vulnerable areas to flash flood hazards in arid regions using remote sensing and GIS-based knowledge-driven techniques. *Nat. Hazards* **2023**, *117*, 2269–2295. [CrossRef]

48. Machiwal, D.; Jha, M.K. Identifying Sources of Groundwater Contamination in a Hard-Rock Aquifer System Using Multivariate Statistical Analyses and GIS-Based Geostatistical Modeling Techniques. *J. Hydrol. Reg. Stud.* **2015**, *4*, 80–110. [CrossRef]
49. Rashash, A.; El-Nahry, A. Rain Water Harvesting Using GIS and RS for Agriculture Development in Northern Western Coast, Egypt. *Geogr. Nat. Disast* **2015**, *5*, 2. [CrossRef]
50. Abdelkareem, M.; Al-Arifi, N. The use of remotely sensed data to reveal geologic, structural, and hydrologic features and predict potential areas of water resources in arid regions. *Arab. J. Geosci.* **2021**, *14*, 704. [CrossRef]
51. Yariyan, P.; Avand, M.; Omidvar, E.; Pham, Q.B.; Linh, N.T.T.; Tiefenbacher, J.P. Optimization of statistical and machine learning hybrid models for groundwater potential mapping. *Geocarto Int.* **2020**, *11*, 2282–2314. [CrossRef]
52. Fewkes, A. The use of rainwater for WC flushing: The field testing of a collection system. *Build. Environ.* **1999**, *34*, 765–772. [CrossRef]
53. Lee, S.; Kim, R. Rainwater Harvesting. In *Encyclopedia of Sustainability Science and Technology*; Springer: New York, NY, USA, 2012; pp. 8688–8702.
54. Kim, R.H.; Lee, S.; Kim, Y.M. Development of rainwater utilization system in Korea. In Proceedings of the 11th IRCSA, Mexico City, Mexico, 25–29 August 2003.
55. Conoco. *Geological Map of Egypt, Scale 1:500,000*; The Egyptian General Petroleum Corporation: Cairo, Egypt, 1987.
56. Mosalem, A.; Redwan, M.; Abdel Moneim, A.A.; Rezk, S. Hydrogeochemical Characteristics of Groundwater from Wadi Asal and Wadi Queih, Quseir, Red Sea, Egypt. *Sohag J. Sci.* **2023**, *8*, 113–117. [CrossRef]
57. Nasr, A.; Abdelkareem, M.; Moubark, K. Integration of remote sensing and GIS for mapping flash flood hazards, Wadi Queih, Egypt. *SVU-Int. J. Agric. Sci.* **2023**, *4*, 197–206. [CrossRef]
58. Dabash, M.H.A. Evaluation of water resources in the area between Quseir–Safaga, Northern Red Sea Coast, Egypt. MSc Thesis, Faculty of Science, Assuit University, Assiut, Egypt, 2004; 180p.
59. Saaty, T.A. scaling method for priorities in hierarchical structures. *J. Math. Psychol.* **1977**, *15*, 234–281. [CrossRef]
60. Obi Reddy, G.P. Evaluation of groundwater potential zones using remote sensing data—A case study of Gaimukh watershed, Bhanadra District, Maharastra. *J. Indian Soc. Remote Sens.* **2000**, *28*, 19–32. [CrossRef]
61. Eastman, J.R. Multi-criteria evaluation and GIS. In *Geographical Information Systems*, 2nd ed.; Longley, P.A., Ed.; John Wiley and Sons: New York, NY, USA, 1996; Volume 1, pp. 493–502.
62. Abdalla, F.; El Shamy, I.; Bamousa, A.O.; Mansour, A.; Mohamed, A.; Tahoon, M. Flash Floods and GroundwaterRecharge Potentials in Arid Land Alluvial Basins, Southern RedSea Coast, Egypt. *Int. J. Geosci.* **2014**, *5*, 971–982. [CrossRef]
63. Abdelkareem, M.; Mansour, A.; Akawy, A. Mapping Groundwater Recharge Potential in the Nile Basin Using Remotely Sensed Data and GIS Techniques. In *Sustainability of Groundwater in the Nile Valley, Egypt*; Springer International Publishing: Cham, Switzerland, 2022; pp. 293–318.
64. Abdekareem, M.; Abdalla, F.; Al-Arifi, N.; Bamousa, A.; El-Baz, F. Using Remote Sensing and GIS-Based Frequency Ratio Technique for Revealing Groundwater Prospective Areas at Wadi Al Hamdh Watershed, Saudi Arabia. *Water* **2023**, *15*, 1154. [CrossRef]
65. Aly, M.M.; Sakr, S.A.; Zayed, M.S.M. Selection of the optimum locations for rainwater harvesting in arid regions using WMS and remote sensing. Case Study: Wadi Hodein Basin, Red Sea, Egypt. *Alex. Eng. J.* **2022**, *61*, 9795–9810. [CrossRef]
66. Kinzelbach, W.; Brunner, P.; Von Boetticher, A.; Kgotlhang, L.; Milzow, C. Sustainable water management in arid and semi-arid regions. In *International Hydrology Series Groundwater Modelling in Arid and Semi-Arid Areas*; Wheater, H.S., Mathias, S.A., Li, X., Eds.; Cambridge University Press: Cambridge, UK, 2010; pp. 119–130. [CrossRef]
67. Schmid, T.; Koch, M.; Gumuzzio, J. Application of hyperspectral imagery to map soil salinity. In *Remote Sensing of Soil Salinization: Impact and Land Management*; Metternicht, G., Zinck, A., Eds.; CRC Press: Boca Raton, FL, USA; Taylor and Francis Publisher: Boca Raton, FL, USA, 2009; Chapter 7; pp. 113–139.